2D-DOA ESTIMATION WITH DIFFERENCE AND SUM COARRAY FOR L-SHAPED DISTRIBUTED ARRAY

Yanping Liao[1], Linlin Hao[2], Yihong Lin[3]

[1,2]Department of Information and Communication Engineering, Harbin Engineering University, Harbin, China
[3] Company Limited of Guangdong OPPO Mobile Telecommunications, OPPO, Guangdong, China
Email: hll@hrbeu.edu.cn

Keywords: DISTRIBUTED ARRAY, L-SHAPED ARRAY, DIFFERENCE AND SUM COARRAY, DEGREE OF FREEDOM, 2-D DIRECTION OF ARRIVAL ESTIMATION.

Abstract

This paper first constructs a novel L-shaped distributed array for two-dimensional (2-D) direction of arrival (DOA) estimation. Based on this, difference and sum coarrays (DSCAs) of the distributed nested array and the improved distributed array are obtained from the spatial and temporal information of the received data. And the closed-form expressions about the sensor locations, DSCA, and degree of freedom (DOF) are derived. The formed virtual array is composed of two orthogonal portions with identical distributed uniform linear arrays. While increasing DOF for the distributed nested array, the improved distributed array achieves a larger continuous aperture. Next, taking average of the repeat elements in the virtual array is equivalent to increasing the number of snapshots, which improves the estimation accuracy. Then, spatial smoothing is performed to restore the rank of each covariance matrix. Finally, the dual-size ESPRIT algorithm is applied to estimate the azimuth and elevation angles, respectively. Simulation results are conducted to demonstrated the effectivity of the proposed method and the high DOF of the improved distributed array.

1 Introduction

Two-dimensional (2-D) direction of arrival (DOA) estimation is a hot research direction in array signal processing, widely applied many areas, such as radar, internet of things, and wireless communication [1]-[3]. Nowadays, many 2-D arrays, such as L-shaped array (LA) [4], planar arrays [5], and parallel array [6], are used for underdetermined 2-D DOA estimation. Among them, LA is more attractive due to simpler configuration and better estimation performance, and many algorithms based on LA are proposed. These algorithms can be divided into two classes. This paper primarily focuses on one class that applies 1-D DOA estimation on each subarray of LA. Traditional 1-D DOA estimation algorithms, such as the subspace-based ESPRIT [7] and MUSIC algorithms [8], primarily rely on uniform linear arrays (ULAs). And the detectable sources are N when ULA is with $N-1$ sensors. In order to obtain higher degree of freedom (DOF) and more accurate DOA estimation, increasing the number of ULA elements is required, leading to higher hardware cost and lower system flexibility.

Sparse arrays with higher DOF were developed. In [9], minimum hole array (MHA) was proposed. It is a kind of sparse arrays with more DOF than ULA, but there are not analytical expressions for array geometry and DOF. In [10], the nested array (NA) composed of two ULAs was proposed, with concise geometry and high DOF, and $O(N^2)$ DOF can be achieved with $O(N)$ physical sensors. To further increase DOF, the augmented nested array (ANA) [11] and the enhanced nested array [12] were proposed. In [13], the distributed array composed of multiple small aperture subarrays was proposed, which can significantly increase the array aperture and the DOA estimation accuracy. To further expand the array aperture, many coarray-based DOA estimation algorithms of 1-D sparse array were proposed. In [10], Piya Pal exploited the signal second-order statistics to increase DOF of the physical array, and spatial smoothing was used to improve the DOA estimation accuracy. In [13], a Vectorized Conjugate Augmented MUSIC (VCAM) algorithm was proposed and the difference and sum coarray (DSCA) was constructed to greatly increase DOF. For distributed arrays, in [15], the distributed nested array (DNA) was proposed, and Khatri-Rao product was used to improve the DOF and resolution of the array. In [16], a weighting signal subspace MUSIC method (WSSMUSIC) based on DNA was proposed to obtain unambiguous estimation.

For LA based on 1-D DOA estimation, in [17], the proposed method, based on cross-correlation matrix, can improve the DOA estimation performance and reduce the computational complexity. In [18], for L-shaped nested array (LNA), Dong *et al.* proposed two methods, while the DOF is discontinuous. In [19], a method for reconstructing the signal covariance matrix in the co-array domain was proposed, which increases the number of detectable sources. In [20], the L-shaped distributed augmented nested array (LANA) and the method by using spatial and temporal information was proposed, which improves DOA estimation accuracy at low signal-to-noise ratios (SNRs). The aforementioned works are based on the difference coarray (DCA), while using DSCA can achieve higher DOF.

To improve DOF and DOA estimation accuracy, a novel L-shaped distributed array and the corresponding method are presented. In this paper, sum and difference operations on

https://doi.org/10.1049/icp.2024.1041

DNA are performed, while the formed virtual array still contains many holes. Hence, an improved distributed array (IDA) is constructed. The final virtual array is composed of two identical ULAs on each axis. Compared to DNA, the consecutive DOF obtained from DSCA is greatly increased. Then the dual-size ESPRIT algorithm with redundancy averaging, which enhance data utilization by averaging repeated elements, is applied to estimate the azimuth and elevation angles, respectively. Simulation results support the validation of the proposed method.

The rest of the paper is organized as follows. Sections 2 introduces system models including novel L-shaped distributed array, signal model, and review of the VCAM algorithm. Section3 introduces 2-D DOA estimation with DSCA including DSCAs of DNA and the improved distributed array, dual-size ESPRIT algorithm with redundancy averaging, and algorithm analysis. Section 4 validates the effectivity of proposed method. Section 5 is the conclusion part.

2 System Model

2.1 Novel L-shaped Distributed Array

As shown in Fig 1(a), DNA consists of two identical two-level NAs with $M = M_1 + M_2$ physical sensors, $d_1 = \lambda/2$ (where λ denotes the wavelength of the signal), and $d_2 = M_1 d_1 + d_1$. The distance between the phase centers of the two subarrays is $D(D \gg \lambda/2)$. The geographies of the two-level NA can be defined as

$$\begin{cases} \mathbb{S}_{NA1} = \{ s_1 \mid s_1 = 1, 2, \ldots, M_1 \} \\ \mathbb{S}_{NA2} = \{ s_2 (M_1 + 1) \mid s_2 = 1, 2, \ldots, M_2 \} \end{cases} \tag{1}$$

From (1), the set of all sensor positions of a two-level NA is $\mathbb{S}_{NA} = \mathbb{S}_{NA1} \bigcup \mathbb{S}_{NA2}$, then the sensor positions of DNA can be denoted as $\mathbb{S}_{DNA} = \mathbb{S}_{NA} \bigcup (\mathbb{S}_{NA} + D)$, and the total number of its sensors is $M' = 2M = 2(M_1 + M_2)$.

As shown in Fig. 1(b), the improved distributed array consists of two identical sparse arrays with M_{new} physical sensors. The relationship between M and M_{new} satisfies $M_{new} = M = M_L + M_R + 1$, where $M_L = \lfloor (M-1)/2 \rfloor$, $M_R = \lceil (M-1)/2 \rceil$. The sensor positions of the sparse array can be defined as

$$\begin{cases} \mathbb{S}_L = (M_L + 1) - n, n \in \mathbb{V}_{21} \\ \mathbb{S}_M = (M_L + 1) n, n \in \mathbb{V}_1 \\ \mathbb{S}_R = (M_L + 1) M_R + n, n \in \mathbb{V}_{22} \end{cases} \tag{2}$$

$$\begin{cases} \mathbb{V}_1 = \{1, 2 \cdots, M_R\} \\ \mathbb{V}_{21} = \{0, M_L\} \\ \mathbb{V}_{22} = \{0, 1, 2, \cdots, M_L\}. \end{cases} \tag{3}$$

where $\mathbb{S}_L$, $\mathbb{S}_M$, and $\mathbb{S}_R$ denote the left, middle, and right subarrays, respectively. From (2) and (3), the set of all sensor positions of the sparse array can be written as $\mathbb{S}_{IA} = \mathbb{S}_L \bigcup \mathbb{S}_M \bigcup \mathbb{S}_R$. Then the sensor positions of the improved distributed array is $\mathbb{S}_{IDA} = \mathbb{S}_{IA} \bigcup (\mathbb{S}_{IA} + D)$ with a total number of $M'_{new} = 2M_{new} = 2M = 2(M_1 + M_2)$.

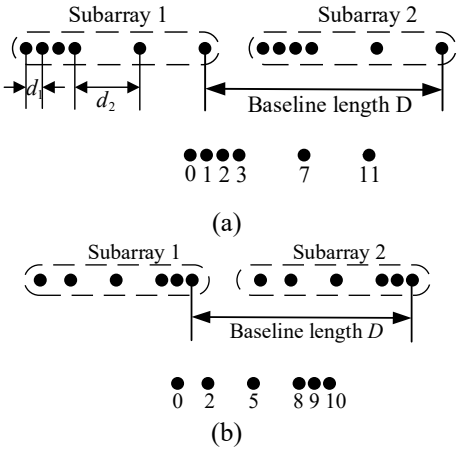

Fig.1 (a) Array configuration of DNA with 12 antennas (b) Array configuration of the improved distributed array with 12 antennas.

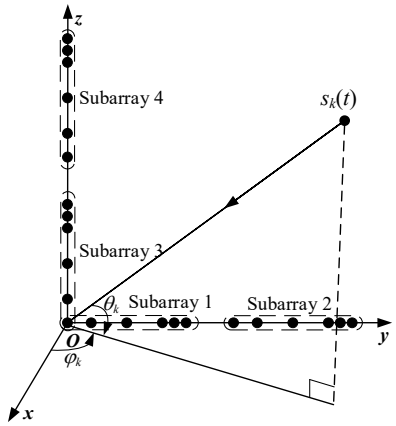

Fig. 2 The physical novel L-shaped distributed array with 23 antennas.

Then, as shown in Fig. 2, the novel L-shaped distributed array is composed of two identical 1-D distributed arrays from Fig. 1(b), placed along the y-axis and z-axis, with the number of sensors in each axis being M' and N'. Define these two subarrays as

$$\begin{aligned} \mathbb{L}_y &= \{ y_1, y_2, ..., y_m \}, m = 1, 2, ..., M' \\ \mathbb{L}_z &= \{ z_1, z_2, ..., z_n \}, n = 1, 2, ..., N' \end{aligned} \tag{4}$$

Apparently, $\mathbb{L}_y = \mathbb{L}_z = \mathbb{S}_{IDA} = \mathbb{S}_{IA} \bigcup (\mathbb{S}_{IA} + D)$.

2.2 Signal Model

Assume K far-field narrowband uncorrelated signals impinging on the array as seen in Fig. 2 from directions $(\theta_k, \varphi_k), k = 1, 2, \ldots, K$, where θ_k denotes the elevation, φ_k denotes the azimuth angle of the k-th signal. The subarray y has M' sensors, the subarray z has N' sensors, and $M' = N' = 2(M_1 + M_2)$. Then, the output of two subarrays $\mathbb{L}_y$ and $\mathbb{L}_z$ at t-th snapshot can be modeled as

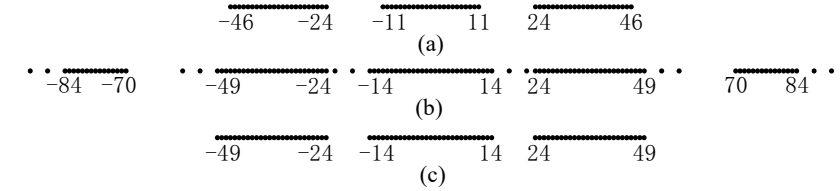

Fig. 3 DSCA of DNA with $(M_1, M_2) = (3,3)$. (a)DCA (b) DSCA (c) Three consecutive parts of DSCA.

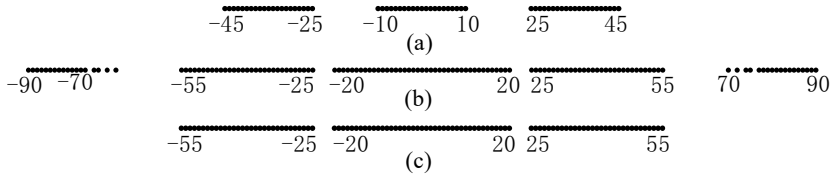

Fig. 4 DSCA of improved distributed array with $(M_L, M_R) = (2,3)$. (a)DCA (b) DSCA (c) Three consecutive parts of DSCA.

$$\boldsymbol{y}(t) = \begin{bmatrix} \boldsymbol{y}_1(t) \\ \boldsymbol{y}_2(t) \end{bmatrix} = \begin{bmatrix} \boldsymbol{A}_{1y} \\ \boldsymbol{A}_{1y}\boldsymbol{\Phi}_y \end{bmatrix} \boldsymbol{S}(t) + \boldsymbol{n}_y(t) = \boldsymbol{A}_y \boldsymbol{S}(t) + \boldsymbol{n}_y(t)$$
$$\boldsymbol{z}(t) = \begin{bmatrix} \boldsymbol{z}_1(t) \\ \boldsymbol{z}_2(t) \end{bmatrix} = \begin{bmatrix} \boldsymbol{A}_{1z} \\ \boldsymbol{A}_{1z}\boldsymbol{\Phi}_z \end{bmatrix} \boldsymbol{S}(t) + \boldsymbol{n}_z(t) = \boldsymbol{A}_z \boldsymbol{S}(t) + \boldsymbol{n}_z(t) \quad (5)$$

where $t = 1, \cdots, T$, and T is the number of snapshots. $\boldsymbol{y}(t)$ and $\boldsymbol{z}(t)$ are receive data vectors of $\mathbb{L}_y$ and $\mathbb{L}_z$ at t-th snapshot, respectively; $\boldsymbol{y}_1(t)$ and $\boldsymbol{z}_1(t)$, $\boldsymbol{y}_2(t)$ and $\boldsymbol{z}_2(t)$ are receive data vectors of the first and second subarrays, respectively. $\boldsymbol{A}_{1y} = [\boldsymbol{a}_{1y}(\theta_1, \varphi_1), \boldsymbol{a}_{1y}(\theta_2, \varphi_2), ..., \boldsymbol{a}_{1y}(\theta_K, \varphi_K)]$ and $\boldsymbol{A}_{1z} = [\boldsymbol{a}_{1z}(\theta_1, \varphi_1), \boldsymbol{a}_{1z}(\theta_2, \varphi_2), ..., \boldsymbol{a}_{1z}(\theta_K, \varphi_K)]$ are the steering vectors of the first subarray, where $\boldsymbol{a}_{1y}(\theta_k, \varphi_k) = [1, e^{\mathrm{j}2\pi y_2 \cos\theta_k \sin\varphi_k / \lambda}, \ldots, e^{\mathrm{j}2\pi y_M \cos\theta_k \sin\varphi_k / \lambda}]^{\mathrm{T}}$ and $\boldsymbol{a}_{1z}(\theta_k, \varphi_k) = [1, e^{\mathrm{j}2\pi z_2 \sin\theta_k / \lambda}, \cdots, e^{\mathrm{j}2\pi z_N \sin\theta_k / \lambda}]^{\mathrm{T}}$. The k-th signal $s_k(t) = A_k e^{\mathrm{j}\omega_k t}$, where A_k is the amplitude of signal, ω_k is the small frequency offset, and $\boldsymbol{S}(t) = [s_1(t), s_2(t), \ldots, s_K(t)]^{\mathrm{T}}$. $\boldsymbol{n}_y(t)$ and $\boldsymbol{n}_z(t)$ are temporarily and spatially white noise vectors with zero-mean and variance σ_n^2. $\phi_{yk} = 2\pi D \cos\theta_k \sin\varphi_k / \lambda$, $\phi_{zk} = 2\pi D \sin\theta_k / \lambda$, $\boldsymbol{\Phi}_y = diag(e^{j\phi_{y1}}, e^{j\phi_{y2}}, ..., e^{j\phi_{yK}})$, $\boldsymbol{\Phi}_z = diag(e^{j\phi_{z1}}, e^{j\phi_{z2}}, ..., e^{j\phi_{zK}})$.

2.3 VCAM Algorithm

For $\mathbb{L}_y$ and $\mathbb{L}_z$, both sensors at positions l_m and l_n, where $m, n = 1, 2, ..., M'$, then the corresponding output data are $y_m(t)$ and $y_n(t)$, $z_m(t)$ and $z_n(t)$. Let $n = 1$, select l_1 for reference. The time average functions are defined as

$$\begin{aligned} R_{y_1^* y_m}(\tau) &= \frac{1}{T}\sum_{t=1}^{T} y_1^*(t) y_m(t+\tau) \\ &= \sum_{k=1}^{K} e^{j2\pi(y_m - y_1) d \cos\theta_k \sin\varphi_k / \lambda} R_{s_k^* s_k}(\tau) \\ R_{z_1^* z_m}(\tau) &= \frac{1}{T}\sum_{t=1}^{T} z_1^*(t) z_m(t+\tau) \\ &= \sum_{k=1}^{K} e^{j2\pi(z_m - z_1) d \sin\theta_k / \lambda} R_{s_1^* s_k}(\tau) \end{aligned} \quad (6)$$

where τ is the time lag and $\tau \neq 0$, $R_{s_1^* s_m}(\tau) = |A_k|^2 e^{j\omega_k \tau}$. Varying m from 1 to M', one can construct two time average vectors as

$$\begin{aligned} \boldsymbol{r}_y(\tau) &= \boldsymbol{A}_y \boldsymbol{r}_s(\tau), [\boldsymbol{r}_y(-\tau)]^* = \boldsymbol{A}_y^* \boldsymbol{r}_s^*(-\tau) = \boldsymbol{A}_y^* \boldsymbol{r}_s(\tau) \\ \boldsymbol{r}_z(\tau) &= \boldsymbol{A}_z \boldsymbol{r}_s(\tau), [\boldsymbol{r}_z(-\tau)]^* = \boldsymbol{A}_z^* \boldsymbol{r}_s^*(-\tau) = \boldsymbol{A}_z^* \boldsymbol{r}_s(\tau) \end{aligned} \quad (7)$$

where $\boldsymbol{r}_y(\tau) = [R_{y_1^* y_1}(\tau), \ldots, R_{y_1^* y_{M'}}(\tau)]^{\mathrm{T}}$, $\boldsymbol{r}_z(\tau) = [R_{z_1^* z_1}(\tau), \ldots, R_{z_1^* z_{M'}}(\tau)]^{\mathrm{T}}$, and $\boldsymbol{r}_s(\tau) = [R_{s_1^* s_1}(\tau), \ldots, R_{s_1^* s_{M'}}(\tau)]^{\mathrm{T}}$.

From (7), we have

$$\begin{aligned} \tilde{\boldsymbol{r}}_y(\tau) &= \begin{bmatrix} \boldsymbol{r}_y(\tau) \\ [\boldsymbol{r}_y(-\tau)]^* \end{bmatrix} = \begin{bmatrix} \boldsymbol{A}_y \\ \boldsymbol{A}_y^* \end{bmatrix} \boldsymbol{r}_s(\tau) \\ \tilde{\boldsymbol{r}}_z(\tau) &= \begin{bmatrix} \boldsymbol{r}_z(\tau) \\ [\boldsymbol{r}_z(-\tau)]^* \end{bmatrix} = \begin{bmatrix} \boldsymbol{A}_z \\ \boldsymbol{A}_z^* \end{bmatrix} \boldsymbol{r}_s(\tau) \end{aligned} \quad (8)$$

Assume that T_s is the pseudo sampling period, N_p is the number of pseudo snapshots. Then, the pseudo-data matrices can be expressed as

$$\begin{aligned} \bar{\boldsymbol{R}}_y &= [\tilde{\boldsymbol{r}}_y(T_s), \tilde{\boldsymbol{r}}_y(2T_s), \ldots, \tilde{\boldsymbol{r}}_y(N_p T_s)] \\ \bar{\boldsymbol{R}}_z &= [\tilde{\boldsymbol{r}}_z(T_s), \tilde{\boldsymbol{r}}_z(2T_s), \ldots, \tilde{\boldsymbol{r}}_z(N_p T_s)] \end{aligned} \quad (9)$$

Then, the covariance matrices of (9) are given as

$$\begin{aligned} \bar{\boldsymbol{R}}_{yrr} &= \frac{1}{N_p} \bar{\boldsymbol{R}}_y \bar{\boldsymbol{R}}_y^{\mathrm{H}} \\ \bar{\boldsymbol{R}}_{zrr} &= \frac{1}{N_p} \bar{\boldsymbol{R}}_z \bar{\boldsymbol{R}}_z^{\mathrm{H}} \end{aligned} \quad (10)$$

Vectorizing $\bar{\boldsymbol{R}}_{yrr}$ and $\bar{\boldsymbol{R}}_{zrr}$, we have

$$\begin{aligned} \boldsymbol{q}_y &= vec(\bar{\boldsymbol{R}}_{yrr}) = \boldsymbol{B}_y \boldsymbol{p}_y \\ \boldsymbol{q}_z &= vec(\bar{\boldsymbol{R}}_{zrr}) = \boldsymbol{B}_z \boldsymbol{p}_z \end{aligned} \quad (11)$$

where $\boldsymbol{p}_y = [|A_{y1}|^4, \cdots, |A_{yK}|^4]^{\mathrm{T}}$, $\boldsymbol{p}_z = [|A_{z1}|^4, \cdots, |A_{zK}|^4]^{\mathrm{T}}$, $\boldsymbol{B}_y = [\boldsymbol{A}_y^{\mathrm{T}}, \boldsymbol{A}_y^{\mathrm{H}}]^{\mathrm{H}} \odot [\boldsymbol{A}_y^{\mathrm{T}}, \boldsymbol{A}_y^{\mathrm{H}}]^{\mathrm{T}}$, and $\boldsymbol{B}_z = [\boldsymbol{A}_z^{\mathrm{T}}, \boldsymbol{A}_z^{\mathrm{H}}]^{\mathrm{H}} \odot [\boldsymbol{A}_z^{\mathrm{T}}, \boldsymbol{A}_z^{\mathrm{H}}]^{\mathrm{T}}$. The k-th column vector of $\boldsymbol{B}_y$ and $\boldsymbol{B}_z$ can be formed as

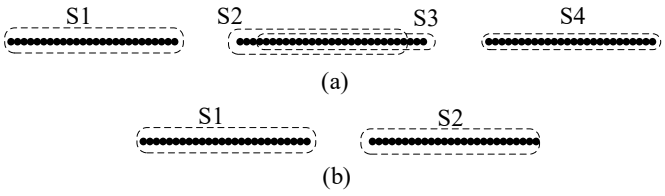

Fig. 5 DSCA of DNA with $(M_1, M_2) = (3,3)$ for DOA estimation. (a) Three consecutive parts. (b) Three identical ULAs with baseline length $D = 35\lambda$.

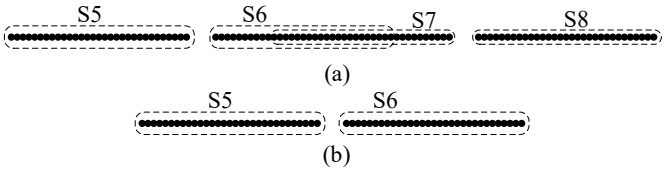

Fig. 6 DSCA of improved distributed array with $(M_L, M_R) = (2,3)$ for DOA estimation. (a) Three consecutive parts. (b) Three identical ULAs with baseline length $D = 35\lambda$.

$$b_{yk} = \begin{bmatrix} \boldsymbol{a}_y(\theta_k,\varphi_k) \otimes \boldsymbol{a}_y^*(\theta_k,\varphi_k) \\ \boldsymbol{a}_y(\theta_k,\varphi_k) \otimes \boldsymbol{a}_y(\theta_k,\varphi_k) \\ \boldsymbol{a}_y^*(\theta_k,\varphi_k) \otimes \boldsymbol{a}_y^*(\theta_k,\varphi_k) \\ \boldsymbol{a}_y^*(\theta_k,\varphi_k) \otimes \boldsymbol{a}_y(\theta_k,\varphi_k) \end{bmatrix}$$
$$b_{zk} = \begin{bmatrix} \boldsymbol{a}_z(\theta_k,\varphi_k) \otimes \boldsymbol{a}_z^*(\theta_k,\varphi_k) \\ \boldsymbol{a}_z(\theta_k,\varphi_k) \otimes \boldsymbol{a}_z(\theta_k,\varphi_k) \\ \boldsymbol{a}_z^*(\theta_k,\varphi_k) \otimes \boldsymbol{a}_z^*(\theta_k,\varphi_k) \\ \boldsymbol{a}_z^*(\theta_k,\varphi_k) \otimes \boldsymbol{a}_z(\theta_k,\varphi_k) \end{bmatrix} \tag{12}$$

3 2-D DOA Estimation with DSCA

As mentioned in section 2, DCA and SCA are obtained through the VCAM algorithm. In this section, an analysis is conducted on the virtual arrays generated by DNA and the improved distributed array, and corresponding expressions of element positions are given. Then, the dual-size ESPRIT algorithm with redundancy averaging is employed to estimate the azimuth and pitch angles respectively, followed by algorithm analysis.

3.1 DSCA of The Improved Distributed Array

With baseline length $D = 35d_1$ and 12 physical sensors, DSCAs are constructed from DNA and the improved distributed array shown in Fig. 1, as depicted in Fig. 3 and Fig. 4, respectively.

It is obvious that DSCA of DNA has more DOF compared to DCA, meaning that VCAM algorithm significantly increases DOF for DNA, but DSCA of DNA still has fewer DOF than IDA. Moreover, for DOA estimation, the continuous portion of the virtual array is used. In this paper, three continuous portions of DNA and IDA are obtained, as shown in Figs. 3(c) and 4(c). However, due to the large baseline length between the two subarrays of the distributed array, the DSCAs of the two subarrays will be discontinuous.

Define that $\mathbb{S}_{DNA\_3U}$ and $\mathbb{S}_{IDA\_3U}$ denote the set of element positions in Fig. 3(c) and 4(c). From (1)-(3) and (12), we have

$$\begin{aligned} \mathbb{S}_{DNA\_3U} &= \mathbb{S}_{DNA\_3U\_L} \cup \mathbb{S}_{DNA\_3U\_M} \cup \mathbb{S}_{DNA\_3U\_R} \\ \mathbb{S}_{DNA\_3U\_L} &= \{-[(M_2+1)(M_1+1)-2]-D, [M_2 \\ &\quad (M_1+1)-1]-D\} \\ \mathbb{S}_{DNA\_3U\_M} &= \{-[(M_2+1)(M_1+1)-2], [(M_2+1) \\ &\quad (M_1+1)-2]\} \\ \mathbb{S}_{DNA\_3U\_R} &= \{-[M_2(M_1+1)-1]+D, [(M_2+1) \\ &\quad (M_1+1)-2]+D\} \end{aligned} \tag{13}$$

$$\begin{aligned} \mathbb{S}_{IDA\_3U} &= \mathbb{S}_{IDA\_3U\_L} \cup \mathbb{S}_{IDA\_3U\_M} \cup \mathbb{S}_{IDA\_3U\_R} \\ \mathbb{S}_{IDA\_3U\_L} &= \{-2[M_2(M_1+1)-2]-D, [M_2 \\ &\quad (M_1+1)-2]-D\} \\ \mathbb{S}_{IDA\_3U\_M} &= \{-2[M_2(M_1+1)-2], 2[M_2 \\ &\quad (M_1+1)-2]\} \\ \mathbb{S}_{IDA\_3U\_R} &= \{-[M_2(M_1+1)-2]+D, 2[M_2 \\ &\quad (M_1+1)-2]+D\} \end{aligned} \tag{14}$$

where $\mathbb{S}_{DNA\_3U\_L}$, $\mathbb{S}_{DNA\_3U\_M}$, and $\mathbb{S}_{DNA\_3U\_R}$ are the left, middle, and right subarrays in Fig. 3(c). $\mathbb{S}_{IDA\_3U\_L}$, $\mathbb{S}_{IDA\_3U\_M}$, and $\mathbb{S}_{IDA\_3U\_R}$ are the left, middle, and right subarrays in Fig. 4(c).

Define that $\mathbb{S}_{DNA\_2U}$ and $\mathbb{S}_{DINA\_2U}$ denote the set of element positions in Figs. 5(b) and 6(b). From (13) and (14), we get

$$\begin{aligned} \mathbb{S}_2 &= \{-[(M_2+1)(M_1+1)-2], [M_2(M_1+1)-1]\} \\ \mathbb{S}_3 &= \{-[M_2(M_1+1)-1], [(M_2+1)(M_1+1)-2]\} \end{aligned} \tag{15}$$

$$\begin{aligned} \mathbb{S}_6 &= \{-2[M_2(M_1+1)-2], [M_2(M_1+1)-2]\} \\ \mathbb{S}_7 &= \{-[M_2(M_1+1)-2], 2[M_2(M_1+1)-2]\} \end{aligned} \tag{16}$$

where $\mathbb{S}_2$ and $\mathbb{S}_3$ denote the set of element positions of the subarrays S2 and S3 in Fig. 5(a), respectively. $\mathbb{S}_5$ and $\mathbb{S}_6$ denote the set of element positions of the subarrays S5 and S6 in Fig. 6(a), respectively. It is observed that there is a distance of $D = 35d_1$ between subarrays S1 and S2, S3 and S4, S5 and S6, and S7 and S8. Therefore, the dual-size ESPRIT algorithm is used for DOA estimation.

DOF of different distributed array structures is shown in Table 1.

Table 1 DOF of different distributed arrays

Array Structure	Consecutive DOF
DNA(DCA)	$6M_2(M_1+1)-3$
DANA(DCA)	$6(M_2+1)(M_1+1)-15$
DNA(DSCA)	$(6M_2+4)(M_1+1)-7$
INA(DSCA)	$10M_2(M_1+1)-17$

3.2 Dual-size ESPRIT Algorithm with Redundancy Averaging

$\boldsymbol{q}_y$ and $\boldsymbol{q}_z$ from (11) are usually needed to remove the repeat elements, but it will reduce data utilization. In this paper, the dual-size ESPRIT algorithm with redundancy averaging is exploited for DOA estimation. By averaging the virtual elements at the same position, it is equivalent to increasing

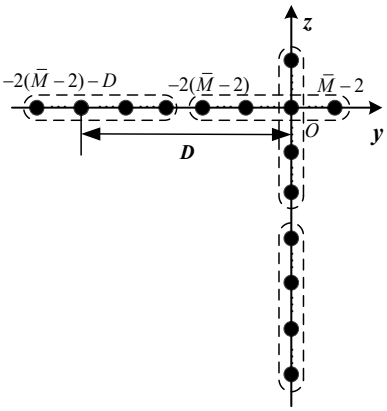

Fig. 7 The formed virtual array.

the snapshots of the received signals, thus enhancing the accuracy of DOA estimation [21].

Due to the influence of SNR and the number of snapshots on $\bar{\boldsymbol{R}}_{yrr}$ and $\bar{\boldsymbol{R}}_{zrr}$, the elements of $\bar{\boldsymbol{R}}_{yrr}$ and $\bar{\boldsymbol{R}}_{zrr}$ corresponding to the same path difference are different, so take the average of the elements corresponding to the same path difference

$$\begin{aligned}\bar{\boldsymbol{q}}_y(dsca_u)&=\frac{1}{w(dsca_u)}\sum_{i=1}^{w(dsca_u)}\boldsymbol{q}_{yi}(dsca_u)\\ \bar{\boldsymbol{q}}_z(dsca_u)&=\frac{1}{w(dsca_u)}\sum_{i=1}^{w(dsca_u)}\boldsymbol{q}_{zi}(dsca_u)\end{aligned}\tag{17}$$

where $dsca_u$ is path difference, $\boldsymbol{q}_{yi}(dsca_u)$ and $\boldsymbol{q}_{zi}(dsca_u)$ respectively represent the i-th equivalent received data corresponding to the same path difference. $w(dsca_u)$ is the total sum of equivalent received data with the same path difference.

Hence, from (14) and (16), we have

$$\begin{aligned}\bar{\boldsymbol{q}}_{y2u}&=\begin{bmatrix}\boldsymbol{A}_{y2u}\boldsymbol{\Phi}_y^*\\ \boldsymbol{A}_{y2u}\end{bmatrix}\boldsymbol{p}_y\\ \bar{\boldsymbol{q}}_{z2u}&=\begin{bmatrix}\boldsymbol{A}_{z2u}\boldsymbol{\Phi}_z^*\\ \boldsymbol{A}_{z2u}\end{bmatrix}\boldsymbol{p}_z\end{aligned}\tag{18}$$

where $\boldsymbol{A}_{y2u}=[\boldsymbol{a}_{y2u}(\theta_1,\varphi_1),\boldsymbol{a}_{y2u}(\theta_2,\varphi_2),...,\boldsymbol{a}_{y2u}(\theta_K,\varphi_K)]$, $\boldsymbol{A}_{z2u}=[\boldsymbol{a}_{z2u}(\theta_1,\varphi_1),\boldsymbol{a}_{z2u}(\theta_2,\varphi_2),...,\boldsymbol{a}_{z2u}(\theta_K,\varphi_K)]$. For convenience, let $\hat{M}=M_2(M_1+1)$, then we have $\boldsymbol{a}_{y2u}(\theta_k,\varphi_k)=(e^{\mathrm{j}\alpha_k})^{\mathrm{T}}$, $\boldsymbol{a}_{z2u}(\theta_k,\varphi_k)=(e^{\mathrm{j}\beta_k})^{\mathrm{T}}$, $\alpha_k=2\pi k\cos\theta_k\sin\varphi_k/\lambda$, $\beta_k=2\pi k\sin\theta_k/\lambda$, $k=[-2(\hat{M}-2),-2(\hat{M}-2)+1,...0,...,\hat{M}-2]$. Therefore, through the above process, two distributed virtual arrays are obtained and placed along the y-axis and z-axis, and each axis consists of two identical ULAs, as shown in Fig. 7.

Let $\bar{M}=3(\hat{M}-2)+1$, divide the virtual subarray 1 into L overlapping subarrays with $\tilde{M}_1$ elements, in which $\tilde{M}_1=\lfloor(\bar{M}+1)/2\rfloor$, $L=\bar{M}-\tilde{M}_1+1$. And the i-th received vector is written as

$$\bar{\boldsymbol{q}}_{1y2ui}=\boldsymbol{A}_{y2ui}\boldsymbol{\Phi}_y^*\boldsymbol{p}_y,\bar{\boldsymbol{q}}_{1z2ui}=\boldsymbol{A}_{z2ui}\boldsymbol{\Phi}_z^*\boldsymbol{p}_z\tag{19}$$

We can get the equivalent covariance matrices $\bar{\boldsymbol{R}}_{1y2ui}=\bar{\boldsymbol{q}}_{1y2ui}*\bar{\boldsymbol{q}}_{1y2ui}^{\mathrm{H}}$ and $\bar{\boldsymbol{R}}_{1z2ui}=\bar{\boldsymbol{q}}_{1z2ui}*\bar{\boldsymbol{q}}_{1z2ui}^{\mathrm{H}}$. Take the average of $\bar{\boldsymbol{R}}_{1y2ui}$ and $\bar{\boldsymbol{R}}_{1z2ui}$, we get two spatially smoothed matrices

$$\bar{\boldsymbol{R}}_{1y2u}=\frac{1}{L}\sum_{i=1}^{L}\bar{\boldsymbol{R}}_{1y2ui}\bar{\boldsymbol{R}}_{1y2ui}^{\mathrm{H}},\bar{\boldsymbol{R}}_{1z2u}=\frac{1}{L}\sum_{i=1}^{L}\bar{\boldsymbol{R}}_{1z2ui}\bar{\boldsymbol{R}}_{1z2ui}^{\mathrm{H}}\tag{20}$$

Similarly, divide the virtual array into L overlapping subarrays and each with $\tilde{M}_2$ elements, in which $\tilde{M}_2=2\lfloor(\bar{M}+1)/2\rfloor$, and the i-th received vector is given as

$$\bar{\boldsymbol{q}}_{2y2ui}=\begin{bmatrix}\boldsymbol{A}_{y2ui}\boldsymbol{\Phi}_y^*\\ \boldsymbol{A}_{y2ui}\end{bmatrix}\boldsymbol{p}_y,\bar{\boldsymbol{q}}_{2z2ui}=\begin{bmatrix}\boldsymbol{A}_{y2ui}\boldsymbol{\Phi}_y^*\\ \boldsymbol{A}_{y2ui}\end{bmatrix}\boldsymbol{p}_y\tag{21}$$

We can get the equivalent covariance matrices $\bar{\boldsymbol{R}}_{2y2ui}=\bar{\boldsymbol{q}}_{2y2ui}*\bar{\boldsymbol{q}}_{2y2ui}^{\mathrm{H}}$ and $\bar{\boldsymbol{R}}_{2z2ui}=\bar{\boldsymbol{q}}_{2z2ui}*\bar{\boldsymbol{q}}_{2z2ui}^{\mathrm{H}}$. Take the average of $\bar{\boldsymbol{R}}_{2y2ui}$ and $\bar{\boldsymbol{R}}_{2z2ui}$, we get two spatially smoothed matrices

$$\bar{\boldsymbol{R}}_{2y2u}=\frac{1}{L}\sum_{i=1}^{L}\bar{\boldsymbol{R}}_{2y2ui}\bar{\boldsymbol{R}}_{2y2ui}^{\mathrm{H}},\bar{\boldsymbol{R}}_{2z2u}=\frac{1}{L}\sum_{i=1}^{L}\bar{\boldsymbol{R}}_{2z2ui}\bar{\boldsymbol{R}}_{2z2ui}^{\mathrm{H}}\tag{22}$$

Then, (20) and (22) are estimated using the dual-size ESPRIT algorithm, and the azimuth and elevation angles are paired by constructing a cross-correlation matrix.

3.2 Algorithm Analysis

The computational complexity of different algorithms is shown in Table 2, in which $M=M'/2$, M' represents the number of elements on each axis.

Table 2 Computational complexity of different Algorithms

Algorithm	Computational Complexity
LDNA in [15]	$8M^2T+1/16M^6+3/8M^5+15/16M^4+1/2M^3$
LNA in [14]	$4MT^2+16M^2T+4M^6+96M^4+32M^3$
LDANA in [20]	$2MT^2+8M^2T+1/16M^6+3/4M^5+9/4M^4-2M^3$
LDNA in [14]	$4MT^2+16M^2T+1/16M^6+9/16M^5+27/16M^4+27/16M^3$
Proposed method	$4MT^2+16M^2T+1/16M^6+3/4M^5+9/4M^4-2M^3$

Due to $T\gg M$, it is evident that the computational complexity of the proposed method is only inferior to LNA in [14]. This is due to the higher DOF of IDA.

4 Simulation Results

In this section, the performance of the improved distributed array and the proposed method will be evaluated using several numerical examples and compared with other existing schemes. The configuration of the novel L-shaped distributed array is shown in Fig. 2. In the following simulations, the number of all L-shaped arrays except for DOF simulation is

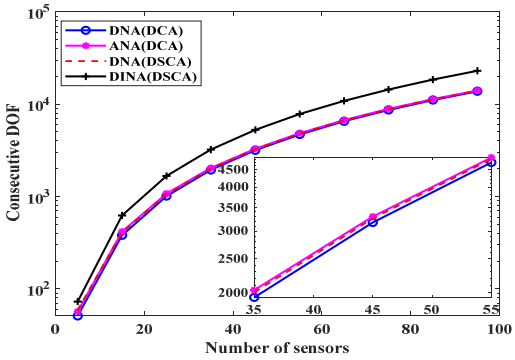

Fig. 8 DOF of virtual arrays versus the number of sensors.

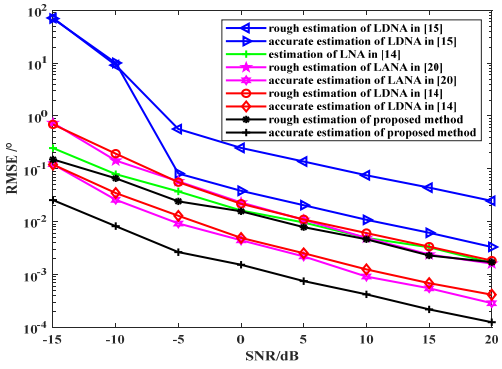

(a)

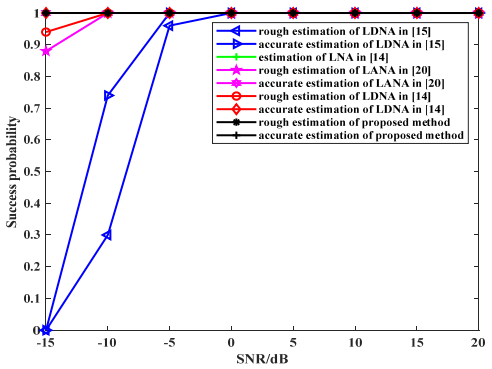

(b)

Fig. 9 (a) RMSE versus SNR (b) Success probability of DOA estimation versus SNR.

23. The root mean square error (RMSE) is used to evaluate 2-D DOA estimation accuracy, which is defined as

$$\mathbf{RMSE}=\sqrt{\frac{1}{JK}\sum_{j=1}^{J}\sum_{k=1}^{K}\left((\hat{\theta}_{k,j}-\theta_k)^2+(\hat{\varphi}_{k,j}-\varphi_k)^2\right)} \quad (23)$$

where J represents the number of Monte Carlo trials and K is the number of sources. (θ_k,φ_k) are elevation and azimuth angles of DOA. $\hat{\theta}_{k,j}$ and $\hat{\varphi}_{k,j}$ denote the k-th estimated elevation angle and azimuth angle in j-th Monte Carlo trials.

The success probability of DOA estimation is defined that the probability of both $|\hat{\theta}_{k,j}-\theta_k|$ and $|\hat{\varphi}_{k,j}-\varphi_k|$ are less than 1°.

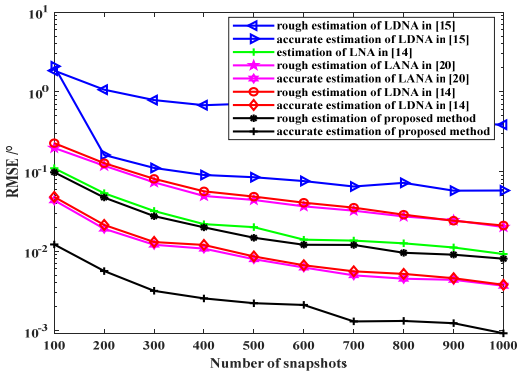

(a)

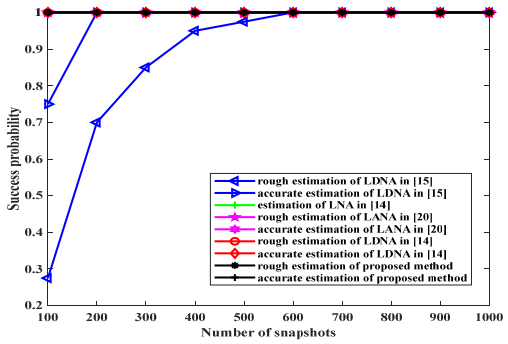

(b)

Fig. 10 (a) RMSE versus the number of snapshots (b) Success probability of DOA estimation versus the number of snapshots.

The probability of target resolution is defined as

$$\begin{aligned}&\left|\hat{\theta}_1-\theta_1\right|,\left|\hat{\theta}_2-\theta_2\right|<\left|(\theta_1-\theta_2)/2\right|\\&\&\left|\hat{\varphi}_1-\varphi_1\right|,\left|\hat{\varphi}_2-\varphi_2\right|<\left|(\varphi_1-\varphi_2)/2\right|\end{aligned} \quad (24)$$

where (θ_1,ϕ_1) and (θ_2,ϕ_2) are the source signals. Corresponding, $(\hat{\theta}_1,\hat{\phi}_1)$ and $(\hat{\theta}_2,\hat{\phi}_2)$ are their estimated values.

4.1 Degree of Freedom

DOF of different distributed arrays listed in Table 1 is compared, with the number of physical sensors varying from 5 to 100. As shown in Fig. 8, it is evident that IDA has the highest DOF. DNA has fewer DOF compared to ANA due to its excessive discontinuous parts in DSCA.

4.2 Estimation Accuracy

4.2.1 RMSE versus Input SNR: Consider one far-field narrowband source from direction $(35^\circ,45^\circ)$, the number of snapshots is $T=2N_p=200$, and the number of Monte Carlo trials is $J=200$. The distance between the phase centers of the two subarrays of each L-shaped distributed array is $D=25\lambda$.

As shown in Fig. 9(a), it is observed that the proposed method achieves the best estimation accuracy over the entire SNR range and maintains excellent estimation performance at

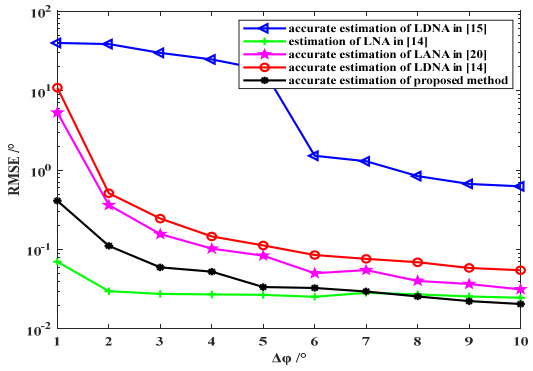

(a)

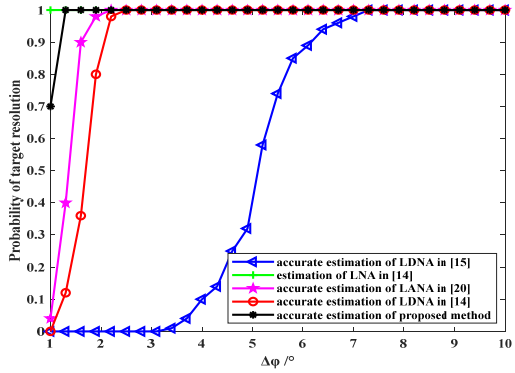

(b)

Fig. 11 (a) RMSE versus $\Delta\varphi$ (b) Probability of target resolution versus $\Delta\varphi$.

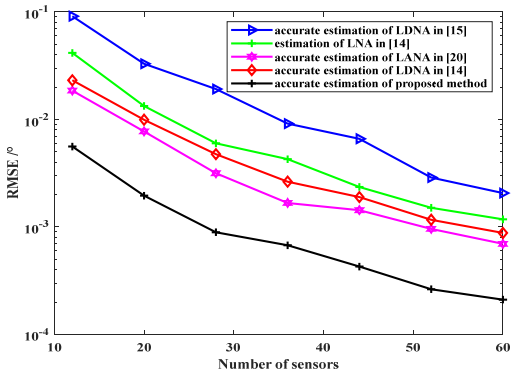

(a)

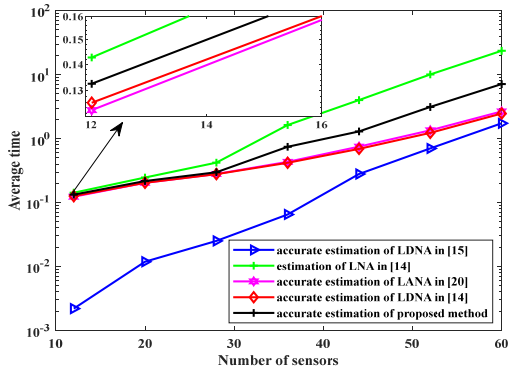

(b)

Fig. 12 (a) RMSE versus the number of sensors (b) Average running time versus the number of sensors.

low SNRs. In Fig. 9(b), only the success probability of the proposed method, the accurate estimation of LDNA in [14], and LNA in [14] reaches 100% when SNR $=-15$dB, while the thresholds for success probability of other algorithms are higher than -15dB. This is due to IDA's high continuous DOF, redundancy averaging operation, and utilization of spatial and temporal information.

4.2.2 RMSE versus The Number of Snapshots: The number of snapshots T varies from 100 to 1000, SNR=-8dB, and the other parameters are the same as in Fig. 9.

As shown in Fig. 10(a), it is obvious that as the number of snapshots increases, the estimation performance of LDNA in [15] remains almost unchanged after T exceeds 400, while the RMSE of other algorithms continues to decrease. The proposed method achieves the best estimation accuracy, and still performs well at small snapshots. In Fig. 10(b), when $T=100$, only success probability of LDNA in [15] lower than 100%.

4.3 Target Resolution

The resolution performance is examined. Consider two far-field uncorrelated signals from $(\theta_1,\varphi_1)=(10^\circ,15^\circ)$ and $(\theta_2,\varphi_2)=(10^\circ+\Delta\varphi,15^\circ+\Delta\varphi)$, where $\Delta\varphi$ is the angular separation varying from 0° to 10°, SNR=-8dB, and $T=200$.

As shown in Fig. 11(a), it is evident that the proposed method and LNA in [14] perform better than the others. The performance of the proposed method is optimal when $\Delta>7^\circ$. In Fig. 11(b), when $\Delta>2.5^\circ$, the success probability of all algorithms, except LDNA in [15], reaches 100%. The proposed method exhibits excellent estimation performance even when the two signals are very close. At this case, it is suitable for the target separation.

4.4 RMSE and Average Running Time versus The Number of Sensors

The performance of various algorithms against sensor number is examined. The number of sensors M' varies from 12 to 60, SNR=-8dB, $T=200$, and the baseline length $D=3[M_2(M_1+1)-2]d_1+10$.

As shown in Fig. 12(a), it is observed that LDNA in [15] performs the worst, while the proposed method exhibits the best performance, mainly due to the proposed method having the largest continuous DOF. In Fig. 12(b), LDNA in [15] has the shortest average running time, which is attributed to its lower DOF. LNA in [14] has the longest average running time because, at the same number of physical sensors, its received data covariance matrix has the largest dimension. The proposed method has a shorter average running time compared to LNA in [14], as it leverages the high degrees of freedom of IDA and exploits spatial and temporal

information, resulting in a relatively larger computational complexity.

5 Conclusion

In this paper, a novel L-shaped distributed array and dual-size ESPRIT algorithm with redundancy averaging are presented to improve DOF of DNA and data utilization of the repeated virtual elements. Two orthogonal identical distributed ULAs can be obtained based on spatial and temporal information of the received data by forming correlation and conjugate correlation data. The continuous DOF is significantly higher than that of DNA, and closed-form expressions of physical sensors, positions of virtual elements, and DOF are provided. Virtual elements in the same locations are averaged, which is equivalent to increasing the number of snapshots. Finally, the dual-size ESPRIT algorithm is exploited to estimate the azimuth and pitch angles respectively, and DOA estimation accuracy is significantly improved. It is worth noting that the proposed method's higher DOF results in increased complexity in the decomposition of the covariance matrix, leading to longer average running time. Further research is needed to address this issue.

6 Acknowledgements

This work was supported in part by the National Major Research and Development project of China under grants 2018YFE0206500.

7 References

[1] H. Krim and M. Viberg: 'Two decades of array signal processing research: The parametric approach', *IEEE Signal Process. Mag.*, 1996, 13, (4), pp. 67–94

[2] H. Wang, L. Wan, M. Dong, K. Ota, and X. Wang: 'Assistant vehicle localization based on three collaborative base stations via SBL-based robust DOA estimation', *IEEE Internet Things J.*, 2019, 6, (3), pp. 5766–5777

[3] M. C. Vanderveen, A.-J. van der Veen, and A. Paulraj: 'Estimation of multipath parameters in wireless communications', *IEEE Trans. Signal Process.*, 1998, 46, (3), pp. 682–690

[4] Y.-Y. Dong, C.-X. Dong, W. Liu, H. Chen, and G.-Q. Zhao: '2-D DOA estimation for L-shaped array with array aperture and snapshots extension techniques', *IEEE Signal Process. Lett.*, 2017, 24, (4), pp. 495–499

[5] M. D. Zoltowski, M. Haardt, and C. P. Mathews: 'Closed-form 2-D angle estimation with rectangular arrays in element space or beamspace via unitary ESPRIT', *IEEE Trans. Signal Process.*, 1996, 44, (2), pp. 316–328

[6] X. Dai, X. Zhang, and Y. Wang: 'Extended DOA-matrix method for DOA estimation via two parallel linear arrays', *IEEE Commun. Lett.*, 2019, 23, (11), pp. 1981–1984

[7] R. Roy and T. Kailath: 'ESPRIT-estimation of signal parameters via rotational invariance techniques', *IEEE Trans. Acoust., Speech, Signal Process.*, 1989, 37, (7), pp. 984-995

[8] R. Schmidt: 'Multiple emitter location and signal parameter estimation', *IEEE Trans. Antennas Propag*., 1986, 34, (3), pp. 276-280

[9] M. Ishiguro: 'Minimum redundancy linear arrays for a large number of antennas', *Radio Sci.*, 1980, 15, (6), pp. 1163–1170

[10] P. Pal and P. P. Vaidyanathan: 'Nested arrays: a novel approach to array processing with enhanced degrees of freedom', *IEEE Trans. Signal Process.*, 2010, 58, (8), pp. 4167-4181

[11] J. Liu, Y. Zhang, Y. Lu, S. Ren and S. Cao: 'Augmented nested arrays with enhanced DOF and reduced mutual coupling', *IEEE Trans. Signal Process.*, 2017, 65, (21), pp. 5549–5563

[12] P. Zhao, G. Hu, Z. Qu, and L. Wang: 'Enhanced nested array configuration with hole-free co-array and increasing degrees of freedom for DOA estimation', *IEEE Commun. Lett*., 2019, 23, (12), pp. 2224–2228

[13] J.E. Nilsson, H. Warston: 'Radar with separated subarray antennas', *2003 Proceedings of the International Conference on Radar (IEEE Cat. No.03EX695)*, Adelaide, SA, Australia, 2003, pp. 194–199

[14] Z. Chen, S. Ren and W. Wang: 'DOA estimation exploiting extended co-array of coprime array', *2016 CIE International Conference on Radar (RADAR)*, Guangzhou, China, Oct. 2016, pp. 1-4

[15] Y. Wang, B. Chen, M. Yang and M. Zheng: 'High accuracy DOA estimation using separated nested array'. *Systems Engineering and Electronic*, 2015, 37, (2), pp. 253-258

[16] Y. Liao, R. Zhao and H. Liu: 'DOA Estimation Method with the Distributed Nested Array', *2018 10th International Conference on Wireless Communications and Signal Processing (WCSP)*, Hangzhou, China, Oct. 2018, pp. 1-6

[17] N. Tayem, K. Majeed, and A. A. Hussain: 'Two-dimensional DOA estimation using cross-correlation matrix with L-shaped array', *IEEE Antennas Wireless Propag. Lett*., 2016, 15, pp. 1077–1080

[18] Y.-Y. Dong, C.-X. Dong, Y.-T. Zhu, G.-Q. Zhao, and S.Y. Liu: 'Two-dimensional DOA estimation for L-shaped array with nested subarrays without pair matching'. *IET Signal Process*., 2016, 10, (9), pp. 1112-1117

[19] Z. Zheng and S. Mu: '2-D Direction Finding With Pair-Matching Operation for L-Shaped Nested Array', *IEEE Commun. Lett.*, 2021, 25, (3), pp. 975-979

[20] Y. Liao, Y. Lin and R. Zhao: '2D-DOA Estimation Using L-shaped Distributed Augmented Nested Array', *2021 13th International Conference on Wireless Communications and Signal Processing (WCSP)*, Changsha, China, Nov. 2021, pp. 1-7

[21] J. Wei, S. Yan and F. Ning: ' Company Limited of Guangdong OPPO Mobile Telecommunications'. *Systems Engineering and Electronic*, 2022, 44, (4), pp. 1069-1077